Bio-optical modelling and Remote Sensing of Inland Waters

CHAPTER 6
Bio-optical modelling of phytoplankton chlorophyll-a

Author
M.W. Matthews*^
*CyanoLakes (Pty) Ltd., Cape Town, South Africa, mark@cyanolakes.com
^Honorary Research Associate, Department of Oceanography, University of Cape Town, Cape Town, South Africa

NON-PRINT ITEMS
Abstract
This chapter provides an overview of current methods for estimating the concentration of chlorophyll-a (chl-*a*) pigment from remotely sensed reflectance measurements made from space, airborne and ground-based instruments. It reviews the fundamental principles of the 'optical pathways' for obtaining chl-*a* concentration information, including absorption, sun induced chl-*a* fluorescence (SICF), and particulate cellular (back)scattering, whilst highlighting the challenges associated with cyanobacteria versus algae as distinct phytoplankton groups; and presents current techniques (algorithms) likely to offer the greatest value with simple, robust implementation. It assesses the utility of available satellite sensors for estimating chl-*a*, and the likely sensitivity of chl-*a* measurements made from space given instrument and bio-physical constraints.

Key Words
Chlorophyll-*a*; remote sensing; bio-optics; phytoplankton; fluorescence; scattering; algae; cyanobacteria

6.1 Introduction

Phytoplankton are the earth's most prolific primary producers occurring in the world's oceans and freshwaters. Although microscopic in size, they have global significance as they produce about half of the oxygen that makes our atmosphere suitable for mammals to breath (Field et al., 1998). They therefore play a critical role in sustaining life on the planet and are of considerable interest to biologists and scientists who study the earth's biogeochemical cycles. Also, considering the vast expanse of the oceans and inland waters, assessing their occurrence and ecology becomes a very challenging task. In inland waters, the need for monitoring is based less on biogeochemical applications and more on management intervention. Increasingly the world's freshwaters are affected by phytoplankton blooms driven by eutrophication that pose a serious nuisance for water managers and the public. Cyanobacteria (and some species of algae) produce deadly toxins which pose a considerable health risk for recreational water users, and for potable water supplies that may be affected (e.g., Codd, 2000). The negative impacts of eutrophication are manifest by dominant algal and cyanobacteria species which reduce biodiversity and degrade water quality. There is therefore a great need for widespread monitoring and surveillance of inland waters focused on cyanobacteria and algal blooms, and remote

sensing methods are proving to be indispensable for this purpose (e.g., Matthews, 2014; Wynne & Stumpf, 2015; Bresciani et al., 2016; Sayers et al., 2016).

Algae and cyanobacteria change the observed light field through absorption, scattering and inelastic processes, such as fluorescence. Bio-optical models are used to describe this interaction, and are used to obtain information at a global scale by taking advantage of space-borne remote sensing instruments that measure the water surface. These instruments measure the light field emerging from oceans and inland waters at the top of the atmosphere. In simple terms, the biological characteristics of phytoplankton cause them to interact with the light field and cause changes in the observed color of the water. Hence the term "ocean color radiometry" became the name of the discipline related to measuring the color of the oceans surface from space, with the primary aim of measuring chlorophyll-a (chl-*a*) from phytoplankton. However, it became possible to observe even small inland water bodies given advances in the ground sampling distance of modern remote sensing instruments (see Chapter 1 for review). Hence the name "water color radiometry" seems like a more appropriate name for the discipline for the 21st century.

Given that phytoplankton are microscopic, single-celled organisms suspended in water, they cannot be directly observed in their natural environment. Rather, the bulk effect of thousands or millions of cells on the water color is what is observed by the human eye or other sensor through the air-water interface. Therefore, their interaction with light might best be described by the theory of single particle optics, in a manner similar to dust particles in the atmosphere. Using single particle optics as a framework for understanding, the primary biological characteristics affecting the way that light interacts with phytoplankton cells are 1) their cell size and shape, 2) their pigmentation, that is, their assembly of colorful pigments that absorb light, and 3) their cellular structure or chemical composition.

From the perspective of Mie theory (often used to describe the interaction of light with single particles in the size range of phytoplankton)[1], these characteristics relate to: 1) the relative size or the area of the particle intercepted by the light field which affects both absorption and scattering; 2) the imaginary refractive index or 'softness' of the cell which is controlled by absorption; and 3) the real refractive index or 'hardness' of the cell which affects scattering. Thus the biological characteristics of a phytoplankton cell displayed through its size, shape, pigmentation and intracellular structure governs how light is absorbed and scattered by the cell.

The principles that apply to a single cell can be extended to a population of polydisperse cells suspended in the three-dimensional water column which give rise to the bulk optical properties (absorption and scattering) of a water body and thus its color (Morel & Bricaud, 1986). However, the color observed by satellite remote sensing, or the estimated bulk absorption and scattering coefficients, can be traced back to the interaction of light at the scale of a single cell. Understanding the microscopic scale of light interaction with a cell

[1] Mie theory describes the interaction of light with a homogeneous spherical particle – for a detailed treatment of Mie theory for modelling how phytoplankton interact with light see Morel & Bricaud (1986).

provides the theoretical foundation into the subject of bio-optical modelling of chl-*a*. Chl-a pigment is of primary interest because it the most suitable proxy for phytoplankton abundance (Huot et al., 2007). It is thus useful to have a sound understanding of phytoplankton and their characteristics in order to understand how bio-optical modelling might be used to estimate chl-*a* that may be used in models for primary production in the world's oceans and freshwaters.

Phytoplankton cells vary considerably in size and shape between species, and in intracellular structure (intracellular occlusions). Cells vary in size from less than 1 μm (picoplankton) to up to 10 mm (macrophytoplankton), although we are mostly concerned here with nanoplankton and microplankton with sizes less than 200 μm. The variation in size over nine orders of magnitude is comparable to the variation of "forest trees to the herbs that grow at their bases" as described by C. S. Reynolds (2006). Their forms vary from single cells (unicells) to grouped cells (coenobia), filaments, and large colonies. Their structure differs considerably between genera with species-specific structure, e.g. silica plates in diatoms, or gas vacuoles in cyanobacteria. Many species of algae are motile and able to migrate vertically in the water column. These differences in size, structure and behavior impact on their bio-optical properties. Additional complexity is introduced when considering that tens to hundreds of species may be present in a water column at various abundance at any one time. The characteristics of the bulk optical signal from phytoplankton is mostly determined by the dominant species or groups present.

With this in mind, this chapter will investigate bio-optical modelling of chl-*a*, the primary indicator of phytoplankton production, and its estimation using various techniques of detection through different 'optical pathways'. An 'optical pathway' as defined here, refers to the path followed by light through a series of interactions with phytoplankton that enables the inference of the concentration of chl-*a* from the measured signal. These pathways are 1) absorption, 2) fluorescence, and 3) phytoplankton backscattering. Measurements directed at different parts of the electromagnetic spectrum focused on these effects act as pathways for estimating the concentration of chl-*a*. The chapter will introduce physical concepts without delving into unnecessary detail, in order to provide a thorough understanding of the biophysical principles used in the estimation of chl-*a* from remote sensing instruments.

The chapter will pay some attention to the differences between prokaryotic and eukaryotic phytoplankton, and the consequences for estimating chl-*a*. Prokaryotic cyanobacteria are abundant in eutrophic freshwaters and in many coastal seas (e.g. the Baltic Sea); thus they are of particular importance in inland and optically complex waters. Given their unique bio-optical properties and behavior, methods for estimating their chl-*a* concentration are sometimes distinct from that of algae (eukaryotes). These differences will be discussed and outlined with reference to each of the optical pathways.

Rather than acting as a review paper[2], the aims of the chapter are firstly, to present an introductory text of the theoretical basis or first principles for quantitatively deriving chl-*a* from remote sensing measurements via the so-called 'optical pathways'; secondly, to identify the challenges associated with its estimation, focusing on the complexities introduced by water constituents other than phytoplankton found in optically complex waters; and thirdly, to present methods that have been used to solve some of these challenges, and discuss the limitations thereof. Thus the chapter does not attempt to review all available algorithms, but rather to highlight the theory behind the estimation of chl-*a* whilst using several examples of algorithms to illustrate the principles at work. This should point to reader towards creative thought regarding improvements in techniques and algorithms, and towards better understanding of bio-optical modelling of chl-*a* concentrations in water. Lastly, the estimated sensitivity of the approaches will be briefly considered in view of the available light signal, along with the constraints imposed by current remote sensing instruments in space.

6.2 Chlorophyll-*a*: the fundamental measure of phytoplankton biomass and production

Chl-*a* is the photosynthetic green pigment present in all photoautotrophic plants and bacteria, including cyanobacteria. It is most often the primary light-harvesting pigment, responsible for capturing most of the energy from sunlight used in photosynthesis. Chl-*a* absorbs light strongly at wavelengths centered in the blue (near 440 nm) and the red (near 670 nm) parts of the light spectrum (Fig. 6.1). This imparts the typical green coloration to natural waters rich in phytoplankton, but the combination of accessory pigments (e.g. carotenoids and phycobilins) alongside chl-*a* at high cell concentrations can produce colors ranging from brown to red (Dierssen et al., 2006). Chl-*a* is one of a group of chl molecules that have similar absorption characteristics that include chlorophyll-*b* and chlorophyll-*c*.

Fig. 6.1. Chl-a absorption spectrum (in vitro). Used with permission from Hout & Babin (2010).

In eukaryotes, that is algae, the chl-*a* molecules are contained and produced within the chloroplast structure. The chl-*a* molecules are embedded in the thylakoid membranes within the chloroplast (Fig. 6.2). Algae typically have one chloroplast, although some species may have several. In prokaryotes, including planktonic cyanobacteria, the thylakoids containing the chl-*a* molecules are contained within the chromatoplasm, the intracytoplasmic membrane towards the periphery of the cell. Prokaryotes lack the typical chloroplast structure found in eukaryotes, as well as other membrane bound organelles.

[2] For reviews see Ruiz Verdú et al., (2008), Kutser (2009), Matthews (2011), Aurin & Diersen (2012), Odermatt et al. (2012), and Blondeau-Patissier et al., (2014), Mouw et al. (2015) and Palmer, Kutser & Hunter, (2015).

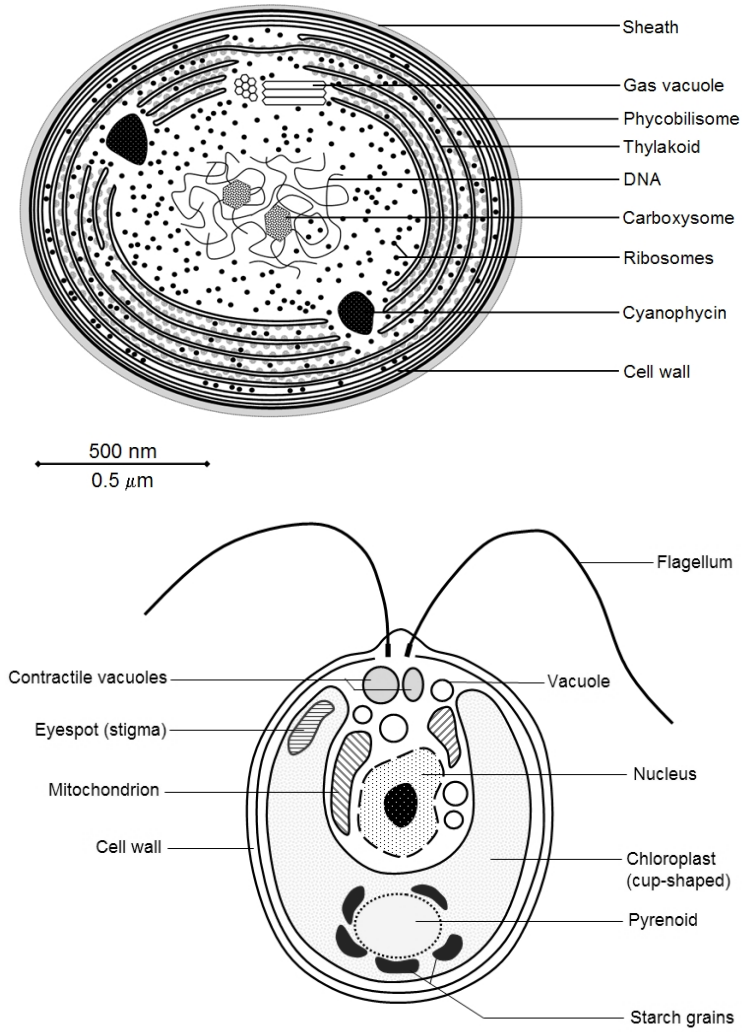

Fig. 6.2. Simplified cellular structure of prokaryotic cyanobacteria (top) and eukaryotic algae (Chlamydomonas) (bottom) showing differences in cellular structure (used with permission from www.cronodon.com).

The packaging of chl-*a* within the cell membrane, and within the thylakoid and/or chloroplast structure has significant optical consequences. Chl-*a* molecules are bound to proteins to form light harvesting complexes that have somewhat different optical properties (Johnsen & Shakshaug, 2007). Larger cells have higher pigment packaging than smaller cells, and thus reduced light absorption per unit chl-*a* (Bricaud et al., 2004; Zhang et al., 2012). The package affect causes the absorption of living cells to be reduced relative to the same pigment concentration in solution (in vitro).

The intracellular chl-*a* concentration, denoted c_i, depends on many factors. These include inherent variations between species, the history of light exposure of the cell and nutrient availability. Thus the value of c_i is neither constant between species, nor in time and space. The average value of c_i for phytoplankton in natural waters is around 5 kg m^{-3}, with typical values varying between 3 and 7 kg m^{-3} (Reynolds, 2006).

Light availability is typically the greatest controlling factor for c_i. In low-light conditions, cells increase their production of light harvesting pigments including chl-*a*, leading to larger c_i values. In contrast lower c_i values are associated with high-light conditions. This is easily observed when culturing phytoplankton in the laboratory, where low-light cultures appear a darker shade of green than high-light cultures. This process is called photoacclimation, regulation of the pigment content to maximize growth rate in a variable light climate (Johnsen & Sakshaug, 2007). The natural variability of c_i poses a challenge for bio-optical models since this factor has a large controlling effect on both absorption and scattering by the cells (Morel & Bricaud, 1986).

Given the ubiquitous nature of chl-*a* in phytoplankton, including algae and bacteria, and its significant positive relationship to phytoplankton biomass (Desortová, 1981), chl-*a* is used globally as a simple measure for phytoplankton in natural waters. Given its relative ease of measurement in the laboratory after extraction in an organic solvent, or direct measurement based on fluorescence in vivo or in vitro, it is routinely measured by government agencies around the world in water quality monitoring programs. In particular, chl-*a* is a vital indicator in programs monitoring the impacts of eutrophication, ecological health status and health risks from harmful cyanobacteria and algal blooms. Therefore, its estimation using remote sensing is of primary interest to water quality management agencies and water utilities. For scientists, when compared to various alternative optical measurements, chl-*a* is the best indicator of the maximum photosynthetic rate (Huot et al., 2007).

6.3 Optical pathways to estimate chlorophyll-*a*

By accurately measuring the changes in the light spectrum using sensitive detectors, the concentration of chl-*a* pigment might be deduced. The following sections addressing the following with respect to each of the optical pathways: the bio-optical properties of phytoplankton; how it can be related to the concentration of chl-*a*; the theoretical basis of measurement; how it is observed in reflectance; the primary methods; complications presented by optically complex waters; approaches for dealing with optically complex waters; and sources of error and likely sensitivity.

6.3.1 Cellular absorption by phytoplankton

The spectral absorption coefficient of phytoplankton (a_{phy}) measured in a spectrophotometer is a combination of absorption from chl-*a* and all associated accessory pigments, and is highly variable in shape (e.g. Fig 6.3). The concentration of chl-*a* is related to a_{phy} at the chl-*a* absorption maxima at 675 nm and 440 nm by a power law function, that has been observed in ocean and inland waters with chl-*a* concentrations over 6 orders of magnitude (0.01 to 10000 mg m^{-3}) (e.g. Bricaud et al., 2004; Gilerson et al., 2010; Matthews & Bernard, 2013; Riddick et al., 2015) (see Fig. 6.4). There is growing evidence that this relationship differs slightly for inland waters (see Riddick et al., 2015). Phytoplankton absorption normalized to chl-*a* (a^*_{phy}) exhibits variability controlled by phytoplankton population size (pigment packaging) and to a lesser degree accessory pigments overlapping the chl-*a* absorption band, particularly affecting the 440 nm band (Bricaud, 1995). An

inverse relationship is observed between ch-*a* and a^*_{phy} caused by the tendency of larger cells to dominate the phytoplankton population size structure at higher chl-*a* concentrations (Bricaud, et al., 2004).

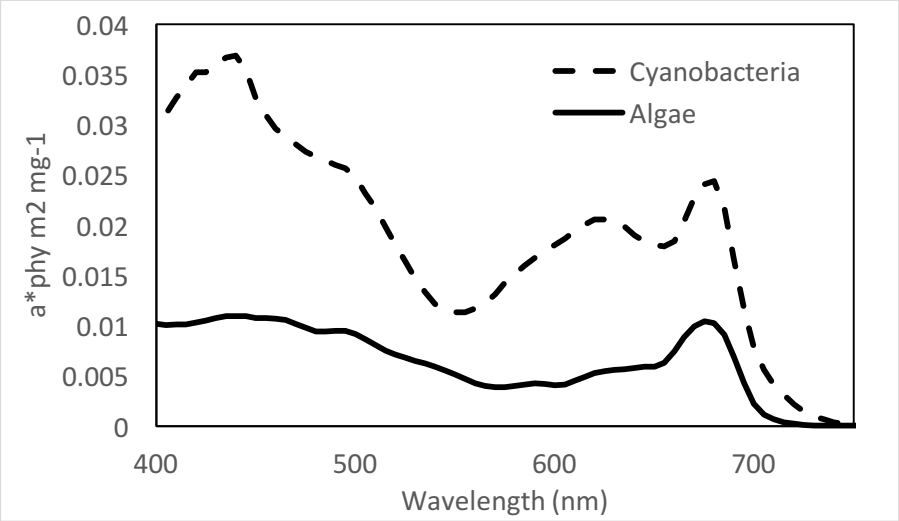

Fig 6.3. Chl-a specific spectral absorption of a cyanobacteria (Microcystis) and an algal (dinoflagellate) species.

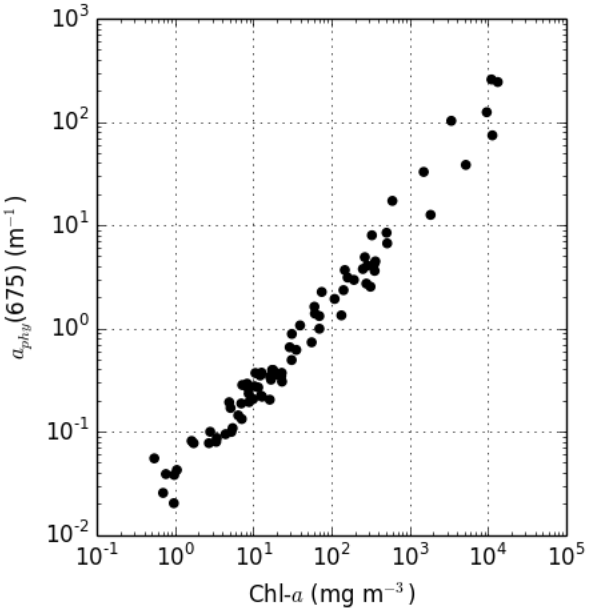

Fig 6.4. $a_{phy}(675)$ versus Chl-a for 3 inland waters in South Africa.

However, in inland waters this relationship may be violated by high abundance of small celled cyanobacteria (e.g., Zhang et al., 2012; Matthews & Bernard, 2015). Thus the conversion from a_{phy} to chl-*a* is more variable in inland waters as dependent upon the phytoplankton size structure and accessory pigment components (which is affected by physiology). Furthermore, the variability in a^*_{phy} (between 0.005 and 0.08 m^2 mg^{-1} at 440 nm) must somehow be accounted for in bio-optical models utilizing the relationship between absorption and chl-*a* concentration (or inherent optical property inversions). One method to do this is to utilize modelled size-specific absorption coefficients (Bernard,

Shillington & Probyn, 2007; Robertson et al., 2014), or to use regional, seasonal, or type-specific parameterizations of the chl-*a* to a^*_{phy} relationship (see Gilerson et al., 2010).

Measuring the intensity of absorption of light by phytoplankton is at first glance the most obvious method for estimating the concentration of chl-*a*. In the laboratory, the pigment is extracted from the sample using various organic solvents, and the subsequent intensity of absorbance centered at the absorption peak and various baselines are measured to calculate the concentration of chl-*a* (e.g. Ritchie, 2006).

This absorption-based approach however poses several challenges for passive spectroradiometers measuring the reflected light spectrum, as against spectrophotometers measuring the loss by absorption and scattering from a beam of light. There are several reasons for this. Firstly, wavelengths coinciding with pigment absorption maxima have fewer photons available for detection by passive sensors. This lowers the signal-to-noise ratio (SNR) in the chl-*a* absorption wavelengths (at 440 and 665 nm). Particularly at high biomass the very small signal increases the error of measurement beyond reasonable limits. In fact, the 665 nm reflectance band is insensitive to larger chl-*a* concentrations (e.g., Gitelson et al., 1999). For this reason, algorithms utilizing blue wavelengths less than ±440 nm are useful only for very low chl-*a* concentrations. For example, Carder (1999) restricted the use of 412 and 440 nm bands to chl-*a* concentrations less than 1.5 mg m^{-3} or 0.025 m^{-1} phytoplankton absorption units. For this reason, at moderate to high chl-*a* concentrations it is more robust from an engineering perspective to measure longer wavelengths or signal from a scattering or inelastic process (discussed below).

A further reason why the absorption pathway is challenging relates to the natural variability in c_i and a^*_{phy} (discussed above). Thus, the conversion from loss of reflectance (caused by absorption) to chl-*a* for cells in vivo is not constant, and results in increased uncertainty. This also applies to inversions retrieving the phytoplankton absorption coefficient, which is used to estimate chl-*a* using the conversion:

$$\text{Chl-}a = \frac{a_{phy}}{a^*_{phy}} \qquad 6.1$$

Despite the practical drawbacks of detecting chl-*a* based on absorption related spectral reflectance features, several highly effective algorithms have been designed on this basis. These approaches most often target effects related to the chl-*a* absorption peak in the blue (near 440 nm), in order to avoid water absorption that affects red wavelengths. The absorption of blue light by increasing concentrations of phytoplankton has been observed in the open ocean as a gradual shift in water color from dark blue to green (e.g., Morel & Prieur, 1977). Thus an empirical algorithm relating the ratio of blue to green light (488 to 551 nm) to chl-*a* concentration is the simplest method of estimating chl-*a* concentration in clear ocean and lake waters (e.g. Carder, 1999, Fig. 6.5).

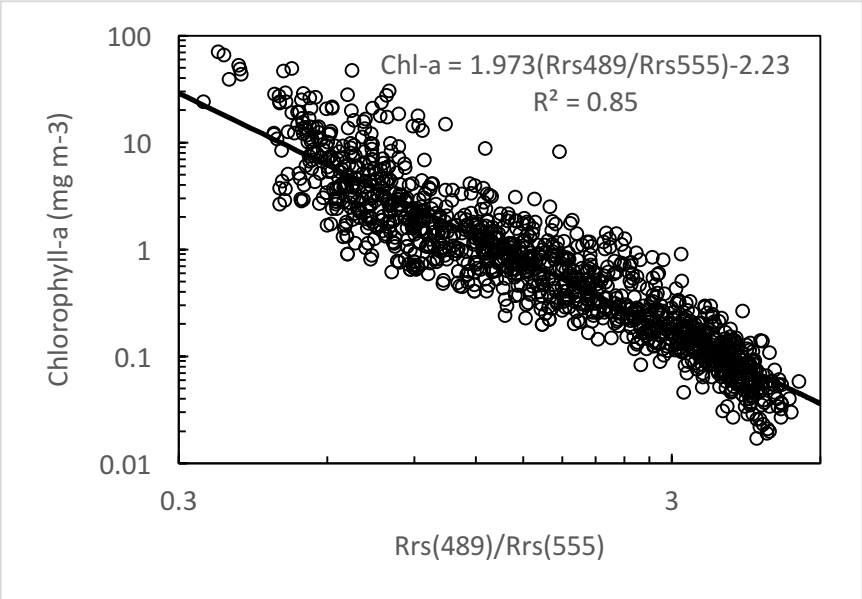

Fig. 6.5. Chl-a versus $R_{rs}(489)/R_{rs}(555)$. Data are used with acknowledgement of the NASA bio-Optical Marine Algorithm Dataset (NOMAD) as cited in Werdell and Bailey (2005).

The most noteworthy examples of this kind of approach are probably the SeaWiFS and MODIS Ocean Color algorithms that utilize several blue/green ratios to maximize the signal-to-noise at selected wavelengths (O'Reilly et al., 1998). This maximum band ratio algorithm is presented here in its configuration for MERIS (OC4Me) from Antoine (2010):

$$\text{Chl-}a = 10^{\wedge}(a_0 + a_1x + a_2x^2 + a_3x^3 + a_4x^4) \quad 6.2$$

where

$$x = \log 10\left(\frac{R_{rs1}}{R_{rs2}}\right) \quad 6.3$$

$$R_{rs1} = \max\left[R_{rs}(443), R_{rs}(489), R_{rs}(510)\right] \quad 6.4$$

and

$$R_{rs2} = R_{rs}(560)$$

$$a_0 = 0.450, a_1 = -3.259, a_2 = 3.523, a_3 = -3.359, a_4 = 0.950$$

The algorithm has proved to be so effective it remains the core algorithm for chl-*a* used for ocean waters for MERIS and OLCI, albeit it's derivation is not purely empirical (Antoine, 2010). These algorithms have been applied globally and remain the benchmark for ocean color and sometimes inland water studies today (see Odermatt et al., 2012; Sayers et al. 2015). Many inland water studies also utilize green/blue ratios in clear lake waters with a good degree of correlation between chl-*a* (e.g., Odermatt et al., 2012; Matsushita et al., 2015).

In optically-complex waters that have significant absorption of either CDOM or particulate matter, the absorption signal in the blue will be the sum of these components (see Chapter 1 and 2 for detailed overview of theory of optical properties of water). In particular, the absorption by humic and fulvic acids is potent across the a_{phy} maximum near 440 nm,

decreasing exponentially towards the red. The absorption properties of tripton (non-living matter) are similar to the exponential function of CDOM but have less steep slopes (see Babin et al., 2003; Binding et al., 2008; Matthews & Bernard, 2013). This causes much uncertainty when solving for the additive total absorption coefficient, and significant ambiguity in solutions given the non-uniqueness (or bijection) of the solution (see Defoin-Platel & Chami (2007) for discussion of ambiguity). Thus the measurement of the effect of phytoplankton absorption on reflectance will have to account for other absorbing substances through the use of a multi-component (additive) bio-optical model. Since the number of unknowns makes the system undetermined, there is no rigorous solution, and iterative processes with empirical laws must be employed (see discussion in Morel & Prieur, 1977).

Because of the influence of these other components, a simple empirical relationship between blue/green wavelengths and chl-*a* becomes severely degraded in waters with high detrital and CDOM absorption (in cases of very dark waters, the signal may be so small as to be unusable). As a result, retrieval of the underlying a_{phy} coefficient is necessary prior to estimation of chl-*a* via inversion of a bio-optical physical model. Studies have therefore focused on the retrieval of a_{phy} (and other constituent absorption coefficients) from reflectance measurements in order to indirectly estimate chl-*a*. These IOP inversion algorithms are focused on the retrieval of the absorption and backscattering coefficients and their parts; the discussion here is limited to those aimed at the estimation of chl-*a* through retrieval of a_{phy}. Estimation of chl-*a* is dependent upon accurate retrieval of a_{phy}, but even if this is achieved the subsequent conversion to chl-*a* will be subject to error (from sources discussed above).

A great number and variety of IOP inversion methods have been suggested such that review here would be protracted and detailed investigations of each technique is beyond the scope of this chapter[3]. The discussion here only highlights some approaches that are useful for further understanding of the complexities of a_{phy} retrieval in inland waters, and for illustrating some of the most promising results for applications.

The reflectance approximation provides a link between reflectance and the IOPs that is commonly used in so-called semi-analytical or algebraic inversion procedures (see Chapter 1 for types of bio-optical models). The observed reflectance is a function of backscattering and absorption $R = f/Q\ (b_b/(a + b_b))$ (Gordon, Brown & Jacobs, 1975). It is worth noting that the *f/Q* factor is subject to uncertainties in highly turbid waters and assumptions from the single scattering approximation (Aurin & Dierssen, 2010; Lee et al., 2011; Piskozub & McKee, 2011). The reflectance approximation is very commonly used as the basis for solutions solving sets of equations from multiple wavelengths for three to four unknowns using linear matrix inversion or nonlinear-least squares optimization. The reflectance can also be expressed in simpler terms ($R \propto b_b/a$) or as a function of K_d (Sathyendranath & Platt, 1997). These semi-analytical approaches typically include various empirical parameterizations or approximations for the IOPs, and sometimes include empirical relationships between reflectance and the IOPs being solved for.

[3] For reviews of IOP inversion algorithms see Gordon, 2002; IOCCG, 2006; Odermatt et al., 2012; Mouw et al., 2015; Li et al., 2013.

These models by necessity make several assumptions regarding the shape and magnitude of a_{phy}, absorption by CDOM and detritus (often combined) and particulate backscattering. Variations is these parameterizations can result is significant differences in algorithm estimates. Some algorithms apply parameterizations in order to account for variability particularly in the shape of a_{phy} based on biomass or regional relationships (e.g. Carder et al., 2004).

It is encouraging that, despite the more extreme constituent concentration ranges and greater variability in IOPs, several IOP inversions have been demonstrated in turbid inland and coastal waters (e.g. Salama et al., 2009; Santini et al., 2010; Aurin & Dierssen, 2012). The quasi-analytical algorithm (QAA) in particular has been parameterized for inland waters (Yang et al., 2013; Mishra, Mishra & Lee, 2014; Pan et al., 2015); however, there has been little examination of the accuracy of chl-*a* estimates from a_{phy}. The simpler inversion model of Li et al. (2013) based on earlier semi-analytical derivations of Gons et al. (2008) and Simis et al. (2007) retrieved chl-*a* from a_t rather than a_{phy}, and shows promising application particularly in high biomass scenarios.

Indirect methods of retrieving the a_{phy} or chl-*a* include alternative non-linear optimization approaches such as spectral decomposition using Gaussian oscillators in phytoplankton rich waters (e.g. Wang et al., 2016), or neural networks (Doerffer & Schiller, 2007), whose estimates of a_{phy} can be correlated to chl-*a* using local parameterizations (e.g. Odermatt et al., 2012). The former is distinct from algebraic semi-analytical inversions in that they do not depend on any knowledge of the IOPs of the water under investigation, but are rather mathematical solutions utilizing synthetic training datasets and statistical methods. The use of the entire spectrum of information by these techniques may lead to advantages over semi-analytical inversions utilizing fewer wavebands.

Having discussed firstly, empirical relationships between reflectance and chl-*a*, and then bio-optical inversions to derive a_{phy} as required in optically complex waters, the reader has a good overview of the main challenges associated with estimating chl-*a* based on absorption related features of reflectance in both clear and complex waters. The reader should keep in mind that the blue /cyan / green spectral region is subject to very low signal in highly absorbing waters, meaning that there are limits as far as the sensitivity of remote sensors is concerned. This poses a constraint on the range over which absorption-based approaches can be expected to perform, from an engineering perspective.

A further challenge arises for absorption-based approaches from atmospheric effects in blue wavelengths (see Chapter 3 for detailed overview of atmospheric correction). Absorbing and scattering aerosols are known to have the greatest effect on blue wavelengths which makes extrapolation of optical thickness estimates from red to blue wavelengths subject to errors, particularly in waters where the signal from NIR wavelengths cannot be assumed to be black as a result of particulate backscattering. Further, spectrally variant bands more than 200 nm apart have significantly differing aerosol attenuation. Thus absorption-related approaches are almost entirely reliant on accurate retrieval of R_{rs} (or the accuracy of coupled air-water models). Further, scattering by stray light into the sensor field of view is significant over

small inland targets, requiring special corrections in spatially constrained waters (this issue also applies to other pathways reviewed here, not only absorption).

From the perspective of sensor design, accurate absorption-based chl-*a* measurements from space demand very high SNRs in precisely placed bands at multiple wavelengths (IOCCG, 1998, 2012). Given its importance for the approach, there is also a need for bands dedicated to atmospheric correction. Since absorption based approaches have defined historical ocean-color missions, these optimal requirements are present in instruments such as SeaWiFS, MODIS, MERIS, VIIRS, OCM, POLDER, OLCI etc. (see Chapter 1 for instruments). However, most of these instruments do not have sufficiently high spatial resolution for inland waters less than approx. 5 km^2. Further, full resolution bands do not have the same sensitivity as reduced resolution bands. Thus, absorption based approaches using lower sensitivity full resolution ocean color datasets on smaller target will not prove as useful or accurate as those used for open ocean waters.

Provided the challenges from atmospheric effects can be sufficiently addressed to derive accurate estimates of R_{rs}, there are clear advantages of utilizing the absorption pathway in clear waters since they allow accurate chl-*a* estimates at very low concentrations less than 0.1 mg m^{-3}. Empirical and semi-analytical blue/green algorithms are likely to provide the highest accuracies for clear oligotrophic waters with chl-*a* less than 10 mg m^{-3}, outperforming the other pathways. The approach is likely to provide the highest accuracy for most of the area of the world's largest inland water bodies (e.g. Great Lakes, African Rift Lakes) since these are typically oligotrophic (e.g. Sayers et al., 2015). Making some assumptions, the absorption-based approach is likely to be applicable for a large portion of the world's inland water surface area (more than 40%[4] larger than 10 km^2).

There are also considerable benefits to be had with coupling absorption approaches with the other pathways in combined or hybrid algorithms that deal with distinct low and high chl-*a* concentration ranges (see Matsushita et al., 2015). In complex and turbid waters, IOP based inversions for the a_{phy} coefficient have been performed with considerable success, however the conversion from a_{phy} to chl-*a* introduces additional uncertainty. IOP inversions incorporating red-wavelength bands provide most promise for higher chl-*a* concentration ranges.

6.3.2 Phytoplankton fluorescence

Part of the light energy that is absorbed by phytoplankton pigments is re-emitted as fluorescence[5] (see Chapter 7 for detailed treatment of fluorescence). The balance of the energy is used in photosynthetic reactions (charge separation) or dissipated as heat through molecular vibrations, known as non-photochemical quenching (NPQ). The processes of fluorescence and NPQ are used to discard excess energy not used in photosynthesis. Pigment-laden light harvesting complexes (LHCs) and chl-*a* molecules contained in photosystems 1 (PSI) and 2 (PSII) absorb light for photosynthesis, a part of which is re-

[4] Based on rough calculation using data in Verpoorter et al. (2014)

[5] For detailed review on algal fluorescence see Huot & Babin (2010) and references therein. For a detailed review on cyanobacteria fluorescence see Campbell et al. (1998)

emitted as photons causing fluorescence. The fluorescence is emitted at a longer wavelength than it is absorbed due to a loss of energy in the process. The chl-*a* molecules contained in the photosystems have different absorption and fluorescence emission characteristics, as these are bound to different protein complexes (Johnsen & Sakshaug, 2007). The great degree of variability in pigment-protein complexes results in significant variability in fluorescence as for absorption (*ibid.*). PSI fluoresces light at wavelengths larger than 700 nm, whilst PSII fluorescence band is centered around 685 nm and at longer wavelengths around 730 to 740 nm.

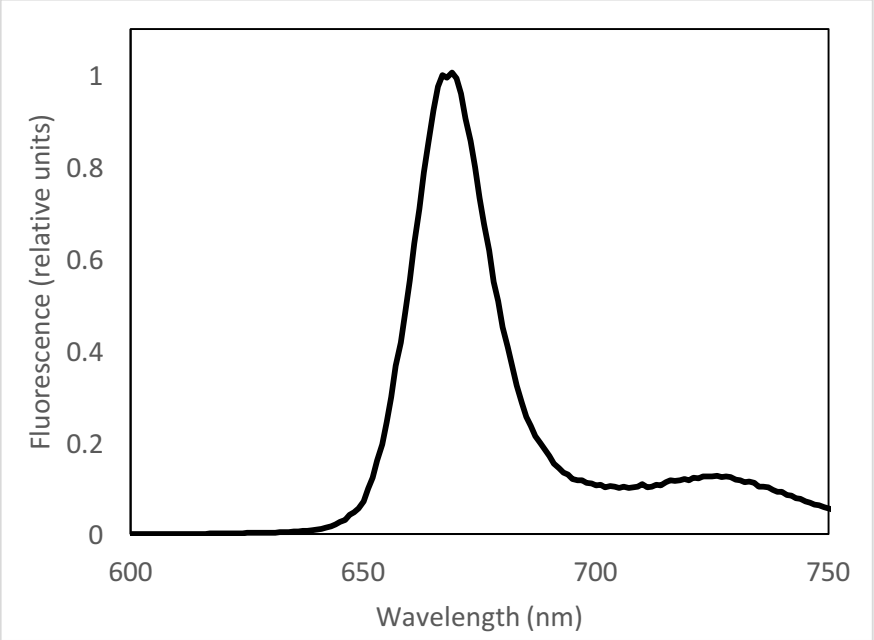

Fig. 6.6. Chlorophyll-a fluorescence emission spectrum (in vitro). Used with permission from Hout and Babin (2010).

In eukaryotic algae, the majority of fluorescence (±95%) arises from photosystem II since this contains the majority of chl-*a* molecules (up to 80%) and the LHCs transfer most of their energy to this photosystem. Thus studies have focused on chl-*a* fluorescence detection in the band centered near 685 nm corresponding to PSII emissions (Fig. 6.6). However, in cyanobacteria, the majority of chl-*a* (>70%) is contained in photosystem I which fluoresces at longer wavelengths (Simis et al., 2012). In addition, the main light harvesting antennae in cyanobacteria are phycobilisomes that contain the pigments phycoerythrin, phycocyanin, and allophycocyanin which transfer electrons to either PSI or PSII. State transitions occur in cyanobacteria causing energy to flow to PSI, thus reducing fluorescence emissions from PSII (Campbell et al., 1998). There is evidence that the phycobilisomes also possess variable fluorescence that overlaps with the chl-*a* fluorescence emission of PS II (Simis et al., 2012). As a consequence, the natural fluorescence signal from cyanobacteria around 685 nm is much weaker than that in algae.

Unlike methods aimed at detecting chl-*a* absorption, fluorescence is an “active” process whereby a detectable signal is emitted from phytoplankton to be measured by a sensor. Estimating chl-*a* from fluorescence signals from PSII is based on the assumption that it is proportional to the concentration of chl-*a* in the cell. In algae, because most of the chl-*a* is contained in photosystem II, this assumption is generally valid. However, this is typically not the case for cyanobacteria as already explained, especially at high concentrations when

significant re-absorption may occur. This conclusion has been supported by observations using in vivo fluorometers and satellite spectroradiometers where limited fluorescence from cyanobacteria has been detected (e.g. Seppälä et al. 2007; Matthews et al., 2012). In fact, a considerable absorption trough exists near 685 nm in the case of cyanobacteria dominant waters (observed by Wynne et al., 2008). Thus the discussion here is generally limited to estimating chl-*a* from algal fluorescence, given that different approaches are required for cyanobacteria (e.g. utilizing PSI emissions, and suitably designed fluorometers, c.f. Simis et al., 2012).

Estimating the concentration of chl-*a* using in vivo fluorescence is routinely used on underway measurement systems (Lorenzen, 1966). These instruments measure the PSII emission in a band near 680 nm under a controlled illumination source as a proxy for chl-*a* concentrations. The theoretical principle, illustrated by Huot & Babin (2010), is that chl-*a* is proportional to fluorescence emitted from PSII provided that the light intensity, chl-*a* absorption, fluorescence quantum yield (proportion of light absorbed to that emitted as fluorescence, typically around 1% (e.g., Gilerson et al., 2007)), and the intracellular fluorescence re-absorption factor are constant (see equation 6 in Huot & Babin, 2010). Given that this is generally not the case with natural samples, in vivo fluorescence only provides a rough estimate of chl-*a* concentration. In vitro estimates of chl-*a* through fluorescence in the laboratory are more accurate as these assumptions are generally valid once chl-*a* is dissolved in an organic solvent such as acetone.

In natural waters phytoplankton also fluoresce strongly in the presence of sunlight, which is known as sun-induced chl-*a* fluorescence or SICF. Studies began investigating whether the SICF signal could be observed in the red wavelengths of upwelling radiance and reflectance measurements. Scientists discovered that the SICF signal was readily observed in reflectance measurements, even at high altitudes using passive airborne spectroradiometers (e.g. Neville & Gower, 1977). SICF is evident in reflectance measurements by a distinct peak near 680 nm, and moving towards longer wavelengths as the phytoplankton concentration increases. The fluorescence emission per unit chl-*a* varies depending on the physiological state of the phytoplankton. The fluorescence peak near 680 nm should not be confused with the red-peak from scattering around 700 nm, which is discussed in detail below.

Using these observations as a starting point, algorithms based on reflectance were developed that targeted the fluorescence line height (FLH) using the same principle as the fluorescence emission peak measurement used in in vivo fluorometry (e.g. Abbott & Letelier, 1999; Gower, Doerffer & Borstad, 1999). Ocean color satellite sensors were configured to detect fluorescence by adding narrow red wavelength bands specifically aimed at the detection of SICF in the oceans (e.g. MODIS, MERIS, OLCI). The FLH measures the height of the reflectance peak caused by SICF and typically has a baseline on either side of the peak centered at the chl-*a* absorption maximum near 665 nm, and the red edge caused by water absorption near 700 nm or 750 nm:

$$FLH = L_1 - L_{baseline}$$

where

$$L_{baseline} = L_0 + (L_2 - L_0) \times \frac{\lambda_1 - \lambda_0}{\lambda_2 - \lambda_0}$$

where *L* is radiance, λ is wavelength, and i=1 is centered on the fluorescence peak.

The FLH itself is of much use for understanding phytoplankton behavior, particularly if an independent estimate of chl-*a* can be simultaneously obtained.

The chl-*a* concentration can be correlated to the FLH from reflectance in natural waters (e.g., Fell et al., 2003; Gons, Auer & Effler, 2008; Matthews et al., 2012; Moreno-Madriñán & Fischer, 2013). Obtaining a consistent relationship between chl-*a* and FLH is based on the same assumptions used in vivo, with the additional constraint dependent on the downward attenuation coefficient, K_d. Since a^*_{phy}, the fluorescence re-absorption factor and the quantum yield vary widely in nature (Fell et al., 2003), FLH provides only a gross index for chl-*a* concentration. The greatest source of uncertainly arises from variability in the chl-*a*:fluorescence ratio (quantum yield) which can readily vary between 0.08 to 0.01 W m^{-2} sr^{-1} um^{-1} per mg chl-*a* (Abbott & Letelier, 1996), enacting variability in the limit of detection of chl-*a* from radiometry. There is some evidence however, that in coastal waters the quantum yield is relatively stable near 1% (Gilerson et al., 2007).

In addition, water turbidity can reduce the sensitivity of FLH algorithms. Variability in K_d in turbid waters not associated with phytoplankton introduces additional uncertainty since it controls the availability of PAR (excitation wavelengths in the blue) and attenuates the upwelling radiance derived from fluorescence. McKee et al., (2007) showed that whilst CDOM absorptions of less than 1 m^{-1} at 440 nm have little effect on FLH, concentrations of mineral particles larger than 5 g m^{-3} cause significant interruption due to enhanced background radiance resulting from particulate scattering. The studies of Gilerson et al. (2007; 2008) confirmed these results showing that attenuation was a more important determinant of fluorescence than the quantum yield factor, and that MODIS and MERIS FLH estimates are significantly degraded by higher concentrations of mineral particulate matter. Thus FLH is most useful in less turbid coastal and inland waters, with lower chl-*a* concentration, or in waters where phytoplankton are optically dominant. The equations relating FLH to the concentrations of chl-*a*, NAP and CDOM absorption developed by Gilerson et al., (2007) may be useful for improving FLH determinations in complex waters.

It is also important to note that whilst FLH signals can be hampered by mineral or particulate backscattering, it is also overwhelmed by phytoplankton backscattering at chl-*a* biomass larger than approx. 20 mg m^{-3}; this is the optical pathway discussed in the next section. Thus from the perspective of inland waters, FLH is appropriate for oligotrophic to mesotrophic waters, but typically not eutrophic waters with chl-*a* larger than ± 20 mg m^{-3} where the scattering signal becomes dominant (for preliminary analysis on the contribution of fluorescence versus scattering see Tao et al., 2013; Gilerson et al. 2008).

FLH algorithms place high demands on instrument spectral sensitivity (SNR) and the precise placement of narrow bandwidths. This means that current FLH estimates from satellite are limited to a few ocean color instruments, such as MODIS, MERIS and OLCI (the FLEX mission will add to this capability along with hyperspectral missions). Encouragingly, application with these instruments has proved to be much use in inland and coastal waters (e.g., Gons, Auer & Effler, 2008; Moreno-Madriñán & Fischer, 2013; Matthews & Odermatt, 2015). In addition

to passive detection, active fluorescence sensing (light detection and ranging - LiDAR) also has promise for chl-*a* retrievals in inland complex waters (e.g. Palmer et al., 2013). There is also evidence that SICF signal in water can be observed in the oxygen absorption band around 760 nm (Lu et al., 2016), as commonly performed in plants (Meroni et al., 2009). Development of methods using this alternative fluorescence signal could improve the use for cyanobacteria populations containing more chl-*a* in PS I and in turbid waters with higher concentrations of suspended sediment.

Atmospheric turbidity also plays a significant role in the sensitivity of FLH algorithms (Abbott & Letelier, 1999). However, given the spectral proximity of the bands used (typically < 100 nm apart), and the baseline peak measurement method, these serve to most often effectively normalize the signal for atmospheric effects, albeit the attenuation from higher concentrations of absorbing aerosols may dampen the FLH signal (*ibid.*). Studies have shown that partial atmospheric corrections accounting only for Rayleigh scattering and absorption, which is more easily performed than aerosol corrections, demonstrate fluorescence signals (Matthews et al., 2012; Matthews & Odermatt, 2015). These recent results accord with the first studies showing that the fluorescence signal was clearly detectable at high altitudes from airborne sensors (Neville & Gower, 1977). Thus, FLH methods do not depend on a full aerosol correction to derive the R_{rs}, which makes application more feasible in complex / bright waters with non-negligible NIR reflectance[6].

In summary, FLH provides a gross estimate of chl-*a* in waters with chl-*a* concentrations between approx. 1 and 20 mg m^{-3}, from sensitive ocean color sensors with high SNR, although the lower limit of sensitivity may be as poor as 8 mg m^{-3} depending on the fluorescence quantum yield, atmospheric and water turbidity. Attenuation in turbid waters reduces the available FLH signal, but preliminary methods already exist to account for the effects of other absorption and scattering components in complex waters (e.g., Gilerson et al., 2008; Lu et al., 2016). The FLH provides a reasonable indication of chl-*a* concentration, with much promise for applications in inland and complex waters.

6.3.3 Phytoplankton scattering

Having explored two direct ways of estimating chl-*a* using absorption and fluorescence, a third indirect method is now considered, that of particulate or phytoplankton backscattering ($b_{b,phy}$). Light scattering by phytoplankton may at it simplest be described by a population of homogeneous spheres using Lorenz-Mie modelling (e.g. Bricaud & Morel, 1986; Stramski et al., 2001). This however is often criticized as being too simplistic, and in particular, of not adequately representing experimentally observed backscattering from phytoplankton (e.g. Volten et al. 1998; Zhou et al., 2012, Whitmire et al., 2010). Alternative two or three layered models providing for additional structures representing a chloroplast or cell wall structure more adequately reproduce observed scattering by phytoplankton (e.g. Quibby-Hunt et al., 1989; Kitchen & Zaneveld, 1992; Quirantes & Bernard, 2006; Matthews & Bernard, 2013). These models may more adequately be used to produce synthetic backscattering coefficients that may be used in modelling studies.

[6] For treatment on atmospheric correction, see IOCCG Report No. 10.

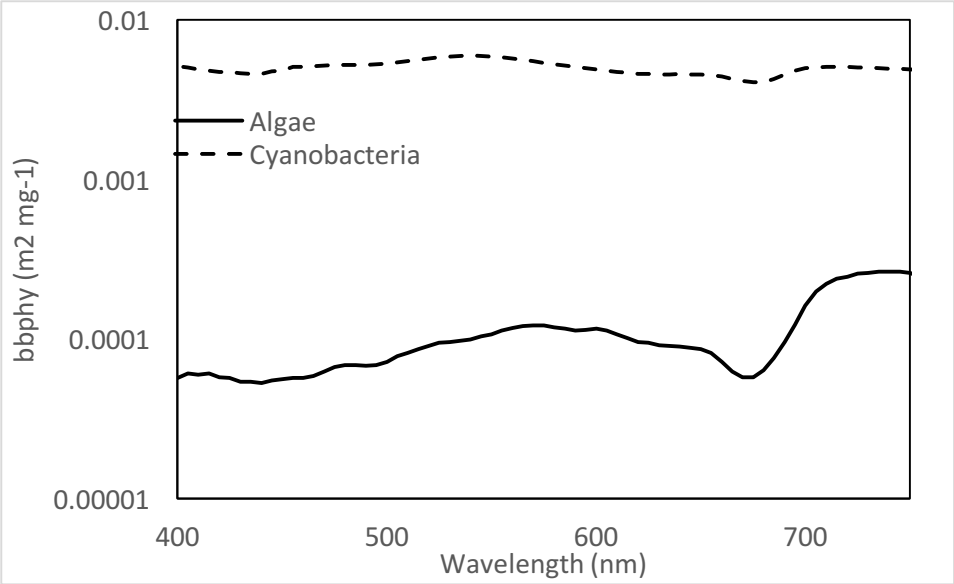

Fig. 6.7. Chlorophyll-a specific backscattering spectra of a cyanobacteria and algal species modelled using a two-layered sphere (from Matthews & Bernard, 2010).

Backscattering spectra of phytoplankton have shapes characteristic of an inverted absorption spectrum with troughs corresponding to the absorption peaks (Fig. 6.7). The magnitude of backscattering varies widely among genera and between species dependent primarily on the cell size (particle size distribution) and cellular structure (real refractive index) of the cells (Svensen, Frette & Erga, 2007; Volten et al., 1998; Witkowski et al., 1998). Cells with considerable structure such as silica cell walls (e.g. diatom frustule), internal gas vacuoles (e.g. cyanobacteria), or scales (e.g. coccolithophores) have considerably higher scattering.

In phytoplankton, the ratio of light scattered in the backward hemisphere to the total scattering coefficient ($\tilde{b}_b$) is typically less than 1% (e.g. Ahn, Bricaud & Morel, 1992; Whitmire et al., 2010; Zhou et al., 2012). Thus phytoplankton generally scatter light poorly in the backward direction. As b_b is directly proportional to the observed reflectance ($R \propto b_b$), it is of primary interest.

According to Mie theory, larger cells exhibit enhanced forward scattering and consequently reduced $\tilde{b}_b$, but this is strongly variable as affected by the real refractive index and the cellular absorption (c_i) (Morel & Bricaud, 1986). This means that scattering varies widely independently of size. For instance, multiple studies present evidence indicating a weak positive relationship between $\tilde{b}_b$ and cell size (Vaillaincount et al., 2004; Whitmire et al., 2010; Zhou et al., 2012), seemingly contradicting the predictions of Mie theory. The enhanced backscattering ratios for larger cells are explained by increasing particulate organic carbon content and internal structures.

In particular, some authors argue for highest backscattering ratios from large dinoflagellates (e.g. Vaillancourt et al., 2004; Whitmire et al., 2010). However, this observation is not presently substantiated by empirical observations of high reflectance values from natural dinoflagellate blooms, and thus may result from bacteria or detached structures in cultures

(see Whitmire et al., 2010). Low reflectance observed in dinoflagellate blooms may on the other hand result from their ability to regulate their position in the water column.

Although the backscattering properties of cyanobacteria are still poorly described, the occurrence of honeycomb-like arrangements of gas vacuoles towards the cell periphery is the cause of dramatically enhanced backscattering observed in cyanobacteria blooms (e.g. Dupouy et al., 2008; Matthews & Bernard, 2013). This scattering which results in high reflectance value can be an important factor for distinguishing cyanobacteria from algae, in addition to their unique pigmentation (e.g. Matthews et al., 2012). The other consequence of vacuoles is that cyanobacteria tend to float on or very near to the surface which has the further impact of increasing brightness. Thus the vertical distribution of cyanobacteria blooms towards the surface in contrast to subsurface algal blooms is also a significant factor resulting in enhanced reflectance values (see Kutser, Metsamaa & Dekker, 2008, for an analysis; see also Chapter 8).

Backscattering normalized to chl-*a* ($b^*_{b,phy}$) ranges four orders of magnitude from 0.02 to 12×10^{-3} m^2 mg^{-1}, for poor and highly scattering species, respectively (e.g. Dupouy et al., 2008, Ahn et al., 1991). The largest values in the literature originate from vacuolate cyanobacteria (Trichodesmium), and algal species (e.g. dinoflagellates) containing unusual cellular structure (but see comment above). In general, small cells scatter more light than large cells per unit chl-*a* (see Vaillancourt et al., 2004). The intracellular chl-*a* concentration (c_i) has a strong influence on $b^*_{b,phy}$ as it normalizes the backscattering according to the number of cells.

There is a strong species-specific relationship between particulate backscattering and the concentration of chl-*a* (e.g. Dupouy et al., 2008, Fig. 3; Whitmire et al., 2010, Fig. 5; Antoine et al., 2011). This relationship is based on the particulate properties of the cells, rather than on any interaction with the pigment itself (absorbing components of the cell)[7]. By way of reason, backscattering is caused by the cell wall and cellular inclusions which include the chloroplast and other cellular structures. Colonial arrangements or coenobium may also impart unique relationships between backscattering and chl-*a*. As the density of cells increases, the particulate backscattering from cellular material increases along with the concentration of chl-*a*.

The relationship between particulate backscattering and chl-*a* concentration has recently been experimentally examined in open ocean waters and may be described by a power law function (Huot et al., 2007; Antoine et al., 2011; Brewin et al., 2012). Whilst is it admitted that $b_{b,p}$ is generally a relatively poor predictor of chl-*a*, the relationship is significant when considering fixed regimes and types. This is evidence that phytoplankton biomass plays a significant role in light backscattering in the oceans, despite the fact that they are presumed to scatter poorly. This holds even for very low biomass which chl-*a* concentrations not exceeding 0.1 mg m^{-3}. It has been deduced that in these conditions material (debris) that co-varies with phytoplankton might be responsible for this relationship, if not the phytoplankton itself (Huot et al., 2007). This relationship has yet to be fully investigated in inland waters.

[7] Although c_i can have a large impact on the intraspecies variability observed in $b^*_{b,phy}$

The principle that chl-*a* is tightly linked to backscattering has been well demonstrated. In meso-eutrophic inland waters with chl-*a* concentrations regularly exceeding 10 mg m^{-3}, the contribution from phytoplankton backscattering to reflectance signals can be overwhelming. This is clearly observable from reflectance measurements made in eutrophic freshwaters that have distinct peaks near 560 and 700 nm from phytoplankton backscattering (see Fig. 6.8). Quibell (1992) noted, based on observations of increases in reflectance from higher concentrations of phytoplankton, that approaches based on algal backscattering should be preferred over those based on absorption effects. This is generally true for water with chl-*a* concentrations exceeding approx. 10 mg m^{-3}. A scattering-based approach to estimating chl-*a* utilizes the peak near 700 nm that becomes apparent at higher concentrations of algae and/or cyanobacteria.

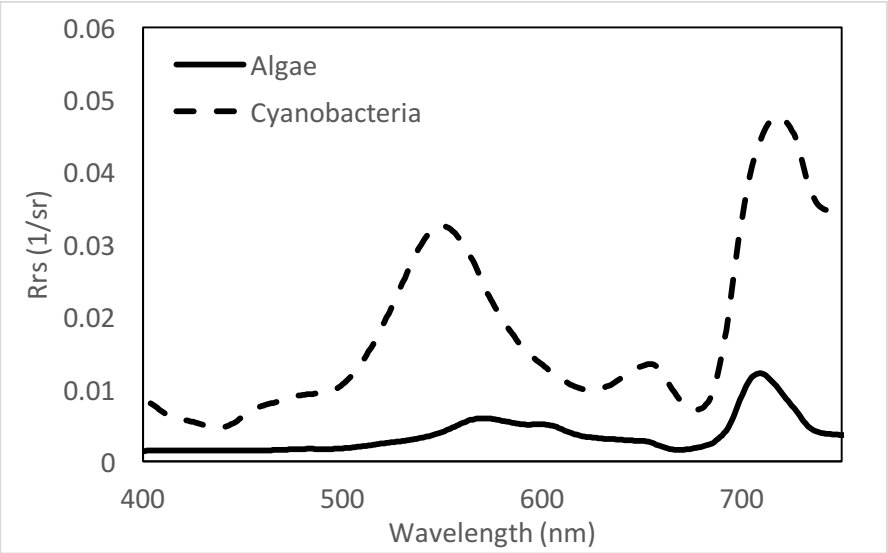

Fig. 6.8. Reflectance spectra from natural populations of vacuolate cyanobacteria (*Microcystis*) and algae (*Ceratium Hirundinelli*) demonstrating red-peak features.

Many similar studies in eutrophic inland waters demonstrate a significant relationship between the red-edge scattering signal near 700 nm and chl-*a* (e.g. Gitelson, 1992; Schalles et al., 1998; Rundquist et al., 1996; Gons , 1999). Chl-*a* is empirically correlated with both the height and position of this peak, which shifts towards increasing wavelengths as biomass increases. This peak results from increased particulate scattering offset by dramatically increasing water absorption at wavelengths larger than 700 nm, and the adjacent chl-*a* absorption band at 665 nm. Fluorescence may also contribute towards the tail of the peak in algae (680 to 690 nm) (Tao et al., 2013), but this is not usually observed in cyanobacteria, which rather has a distinct trough in the fluorescence band around 680 nm, characteristic of re-absorption or state transition effects (Wynne et al., 2008; Matthews et al., 2012).

The scattering peak near 700 nm is preferred over that near 560 nm because of the influence of variable absorption from accessory pigments (e.g. carotenoids), and residual CDOM absorption at shorter wavelengths. In highly absorbing waters with very high phytoplankton biomass and/or CDOM there is typically very little light leaving the water in the blue. Thus red-wavelength approaches provide more useable signal, despite the

relatively high absorption by water, and the low depth of light penetration into the water (which at high biomass may only be a few centimeters). For this reason, the red-peak is most useful in well-mixed eutrophic water bodies, since it neglects the vertical distribution of phytoplankton. Red-wavelengths are also less prone to errors from atmospheric aerosol scattering than blue wavelengths, and techniques such as band ratios or peak height subtraction / derivatives have the advantage of effectively normalizing for atmospheric effects. There is evidence that even uncorrected top-of-atmosphere signals at 700 nm provide a good estimation of chl-*a* (e.g., Giardino et al., 2005; Matthews et al., 2010).

Similar to how the backscattering to chl-*a* relationship is species specific, the chl-*a* versus reflectance red peak height also displays specific relationships by genera (diatoms appear to be the most distinctive type) (Gitelson et al., 1999; Matthews & Bernard, 2013). The location of the red peak is also more consistent between genera than that of the peak near 560 nm, due to variable accessory pigmentation (Gitelson et al., 1999). Recent research has indicated that the chl-*a* specific absorption coefficient, and the fluorescence quantum yield significantly affects the shift in the peak position to longer wavelengths, with the result that various species possess unique relationships between peak position and height and chl-*a* (see Tao et al., 2013). The ability to model unique red-peak behavior resulting from species-specific backscattering and / or fluorescence effects presents an opportunity for distinguishing species based on peak height and position models, particularly in conjunction with accessory pigment related features (e.g. Tao et al., 2013, 2015).

Red-peak scattering based algorithms may form simple reflectance ratios (e.g. 700/665 nm), more complex ratio forms (e.g. three band / four band variants), the normalized difference chlorophyll index (NDCI) (Mishra & Mishra, 2012), and also peak height models (e.g. the reflectance line height (Dierberg & Carriker, 1994); scattered line height (Schalles et al., 1998); the maximum chlorophyll index (MCI) (Gower et al., 2005); the maximum peak height (MPH) (Matthews et al., 2012); and the adaptive reflectance peak height algorithms (Ryan et al., 2014)). These empirical relationships can also be derived using radiative transfer models of reflectance utilizing the species-specific chl-*a* specific phytoplankton absorption and backscattering coefficients (e.g. Matthews & Bernard, 2013; Tao et al., 2013).

The simple two band model (using MERIS bands) is:

$$\text{Chl-}a \propto \frac{R_{rs}(708)}{R_{rs}(665)}$$

The three-band model (using MERIS bands) is:

$$\text{Chl-}a \propto \left(R_{rs}(665)^{-1} - R_{rs}(708)^{-1}\right) \times R_{rs}(753)$$

The NDCI is written as follows (using MERIS bands):

$$\text{Chl-}a \propto \frac{R_{rs}(708) - R_{rs}(665)}{R_{rs}(708) + R_{rs}(665)}$$

Various relationships (e.g. linear, quadratic, power-law, etc.) are used to correlate the concentration of chl-*a* with these variables.

The MPH algorithm searches for the position and height of the peak in the red between 680 and 750 nm, and is formulated for MERIS as follows (Matthews & Odermatt, 2015):

$$MPH = R_{max} - [R_0 + (R_1 - R_0) \times \frac{\lambda_{max} - \lambda_0}{\lambda_1 - \lambda_0}]$$

where

$$R_{max} = \max [R_{681}, R_{709}, R_{753}]$$

and where 0 = 665 nm, 1 = 885 nm, and R is ideally bottom-of-Rayleigh Reflectance.

The MPH principle can be applied to any sensor provided there are sufficient bands in the red. The MPH uses separate chl-*a* algorithms for cyanobacteria and algae dependent upon the identification of specific spectral features related to cyanobacteria.

It is also worth noting that the FLH algorithm has been used to indirectly measure the height of the 709 nm peak, or more directly the depth of the absorption trough at 681 nm (e.g. Palmer et al., 2014; Ampe et al., 2014). This results in a negative value which may be highly correlated with the concentration of chl-*a*. It is likely not appropriate to refer to FLH in these instances, since the lack of signal is not from fluorescence, but is related rather to scattering and absorption effects. This applies particularly to cyanobacteria-dominant waters which replace the fluorescence peak at 681 nm with a distinctive trough (Wynne et al., 2008; Matthews et al., 2012), where it has been referred to as the cyanobacteria index (CI) (Lunetta et al., 2015; Tomlinson et al., 2016).

In complex waters red-peak algorithm are negligibly affected by CDOM because of the spectral distance from blue absorption wavelengths. Variability in suspended sediment concentrations (deposited organic matter, clay and silt) are therefore likely to be the greatest source of error for these algorithms. Most sediment (perhaps with the exception of iron rich sediment) scatter light in a spectrally-invariant manner or with a gently sloping power law function dependent upon the particle size and refractive index (e.g. Stramski et al., 2007). Measured reflectance from sediment suspended in pure water do not exhibit a red peak at 700 nm the way phytoplankton do, due to the lack of a proximal absorption band at 665 nm (Quibell, 1992; Han et al., 1994; Hunter et al., 2008). The effect of sediment is primarily an increase in the magnitude of reflectance across the spectrum. Thus the red peak, which is very much determined by the chl-*a* absorption near 665 nm, is resilient (within limits) to variable suspended sediment concentrations (*ibid.*), and is therefore suitable for providing chl-*a* estimates in highly turbid coastal waters (see Kobayashi et al., 2011). Variations of the reflectance ratio algorithms have been developed to account for the effects of suspended sediment with some success, such as that of Gons et al., (1999), which is based on the reflectance approximation; that of Gitelson et al. (2003) which uses additional NIR band to account for scattering; and the four band model (Le et al., 2009).

A further case which presents a challenge to algorithms making use of red / NIR wavelengths is the case of optically shallow waters with sandy bottoms or submerged aquatic vegetation (SAV). These may exhibit red peaks (e.g. Hill et al., 2014) and are an

additional potential source of error when applying red-peak algorithms to satellite data in inland waters and shallow seas, particularly in areas adjacent to the shore. A method has been developed to flag out waters adjacent to the shore utilizing features in the red (see Matthews & Odermatt, 2015).

All things considered, the sources of error to red-peak derivations of chl-*a* can be summarized as being from variability in $b^*_{b,phy}$ and a^*_{phy}; to a lesser extent variability in the fluorescence quantum yield; scattering from suspended sediment; residual aerosol effects; and the presence of SAV and bottom effects. The likely sensitivity of red-peak / scattering approaches is limited to concentrations greater than approx. 10 mg m^{-3} at which biomass the red peak from scattering becomes apparent. It is important to note that most ocean color sensors lack a suitable narrow band near 710 nm for application of red-peak algorithms from satellite, making MERIS and OLCI particularly useful in eutrophic inland waters. In this respect future hyper/multispectral sensors (such as HICO) can fill an important gap for inland waters requiring higher spatial resolution. However, SNR remains problematic for many hyperspectral sensors (Kudela et al., 2015).

Scattering-based approaches using the red peak have the advantage of spectral proximity, and greater signal from typically higher biomass waters, for atmospheric correction. In this respect, red peak height approaches (MPH, MCI) provide the same advantages presented by FLH, and therefore can be more easily applied with partial atmospheric corrections, such as the bottom-of-Rayleigh reflectance (e.g. Matthews et al., 2012; Lunetta et al., 2015).

6.4 Conclusion

This chapter has provided an overview of the three pathways for estimating chl-*a* from remotely sensed measurements of the reflectance from natural waters. This should give the reader a better appreciation of the first principles involved in the estimation of chl-*a*, as well as an overview of the methods and applications of each approach. The three pathways discussed above represent alternative, complimentary, and sometimes divergent approaches to estimating chl-*a* from reflectance. Each pathway has its own set of advantages and weaknesses, limitations and constraints, and optimal conditions for use. Chapter 7 discussed fluorescence and its measurement and relationship to chl-*a* for readers requiring a more in-depth text.

Absorption approaches are optimal for oligotrophic waters with chl-*a* concentrations less than 5 mg m^{-3} due to the higher sensitivity than the other pathways at this biomass range. The available signal in the blue is reduced by higher concentrations of phytoplankton, and by CDOM and NAP absorption, and atmospheric interference remains a principal source of uncertainty. Fluorescence, whilst subject to wide variability due to physiology, and the influence of attenuation, provides a robust gross index for chl-*a* in the range 1 to ±20 mg m^{-3}. A significant advantage is that FLH provides an effective atmospheric correction. The scattering approach is limited to concentrations above ±10 mg m^{-3}, and is likely the most robust method for estimating chl-*a* concentrations above 20 mg m^{-3}, taking into account the higher relative signal from increasing biomass in the red (for additional sensitivity analysis on ranges of constituent concentrations and chl-*a* see Odermatt et al., 2012). Peak-height calculations can also have the same advantages for atmospheric correction as the FLH. The

development of hybrid approaches, such as combined absorption-scattering (Matsushita et al., 2015), and fluorescence-scattering approaches (Matthews et al., 2012) can optimize performance over wider biomass ranges. The optimal model for chl-*a* retrieval for inland and complex waters (yet to be developed) will probably combine all three approaches (absorption-florescence-scattering), with switching dependent on prior water type classification (e.g. Moore et al., 2014) or species-specific feature detection (e.g. Tao et al., 2015).

There are several areas for future research that will reduce uncertainty for chl-*a* estimates in complex waters. Better understanding of the fine resolution red features of backscattering from algae and cyanobacteria will enhance scattering algorithms (i.e. detailed measurements of the volume scattering function); further assessment of fluorescence variability, and attenuation effects will improve FLH corrections applied to turbid waters; better characterization of variables such as c_i, and further refinement of semi-analytical inversions will enhance absorption-based retrievals in complex waters.

It is clear that estimation of chl-*a* from space requires high thresholds for instrument sensitivity (SNR) (e.g. Hu et al., 2012; Moses et al., 2012) and precise placement of narrow spectral bands. The consequence is that only a few ocean color sensors are suitable for quantitative chl-*a* retrieval over its full scale of variability (0.01 to 10 000 mg m m^{-3}), which is likely to continue to be the case in future. From the perspective of inland waters, the implication is that, for water bodies less than 2 km^2, systematic quantitative chl-*a* estimation is likely to remain something for the future. However, current higher resolution sensors (e.g. Sentinel-2) can offer a partial solution in the interim. The outlook certainly indicates that in inland waters, provided that suitable instruments remain in space, chl-*a* estimates will continue to improve as these methods mature into generally accepted best-practice science, offering considerable advantages for use in a wide range of practical applications. These include services for monitoring threats from cyanobacteria blooms for recreational users and public authorities; systematic wide-scale monitoring of the impacts of eutrophication; and global assessments of lake bio-geochemistry and the long-term impacts of climate change on lake environments.

References

Abbott, M.R. & Letelier, R.M., 1999. *Algorithm Theoretical Basis Document Chlorophyll Fluorescence (MODIS Product Number 20)*, NASA.

Ahn, Y.H., Bricaud, A. & Morel, A., 1992. Light backscattering efficiency and related properties of some phytoplankters. *Deep-Sea Research*, 39, pp.1835–1855.

Ampe, E.M. et al., 2014. A Wavelet Approach for Estimating Chlorophyll-A From Inland Waters With Reflectance Spectroscopy. *Geoscience and Remote Sensing Letters, IEEE*, 11(1), pp.89–93.

Antoine, D., 2010. *Sentinel-3 optical products and algorithm definition. OLCI Level 2 Algorithm Theoretical Basis Document: Ocean Colour Products in case 1 waters*, Available at:

https://sentinel.esa.int/documents/247904/349589/OLCI_L2_ATBD_Ocean_Colour_Products_Case-1_Waters.pdf.

Aurin, D. A. & Dierssen, H. M., 2012. Advantages and limitations of ocean color remote sensing in CDOM-dominated, mineral-rich coastal and estuarine waters. *Remote Sensing of Environment*, 125, pp.181–197.

Babin, M. et al., 2003. Variations in the light absorption coefficients of phytoplankton, nonalgal particles, and dissolved organic matter in coastal waters around Europe. *Journal of Geophysical Research-Oceans*, 108(C7)(3211), pp.4.1–4.20.

Bernard, S., Shillington, F.A. & Probyn, T.A., 2007. The use of equivalent size distributions of natural phytoplankton assemblages for optical modeling. *Optics Express*, 15(5), pp.1995–2007.

Binding, C.E. et al., 2008. Spectral absorption properties of dissolved and particulate matter in Lake Erie. *Remote Sensing of Environment*, 112(4), pp.1702–1711.

Blondeau-Patissier, D. et al., 2014. A review of ocean color remote sensing methods and statistical techniques for the detection, mapping and analysis of phytoplankton blooms in coastal and open oceans. *Progress in Oceanography*, 123, pp.123–144.

Bresciani, M. et al., 2016. Earth observation for monitoring and mapping of cyanobacteria blooms. Case studies on five Italian lakes. *Journal of Limnology*, pp.1–18.

Bricaud, A. & Morel, A., 1986. Light attenuation and scattering by planktonic cells: a theoretical modeling. *Applied Optics*, 25(4), pp.571–580.

Bricaud, A. et al., 1995. Variability in the chlorophyll-specific absorption coefficients of natural phytoplankton: Analysis and parameterization. *Journal of Geophysical Research*, 100(C7), pp.13321–13332.

Bricaud, A. et al., 2004. Natural variability of phytoplanktonic absorption in oceanic waters: influence of the size structure of algal populations. *Journal of Geophysical Research*, 109(C11010), pp.1–12.

Campbell, D. et al., 1998. Chlorophyll fluorescence analysis of cyanobacterial photosynthesis and acclimation. *Microbiology and Molecular Biology Reviews*, 62(3), pp.667–683.

Carder, K.L. et al., 2004. Performance of the MODIS semi-analytical ocean color algorithm for chlorophyll-a. *Advances in Space Research*, 33(7), pp.1152–1159.

Codd, G.A., 2000. Cyanobacterial toxins, the perception of water quality, and the prioritisation of eutrophication control. *Ecological Engineering*, 16(1), pp.51–60.

Defoin-Platel, M., & Chami, M., 2007. How ambiguous is the inverse problem of ocean color in coastal waters? *Journal of Geophysical Research*, 112(C03004), pp.1–16.

Desortová, B., 1981. Relationship between chlorophyll-a concentration and phytoplankton biomass in several reservoirs in Czechoslovakia. *Int. Revue ges. Hydrobiol.*, 66(2), pp.153–169.

Dierssen, H. et al., 2006. Red and black tides: Quantitative analysis of water-leaving radiance and perceived color for phytoplankton, colored dissolved organic matter, and suspended sediments. *Limnology and Oceanography*, 51(6), pp.2646–2659.

Doerffer, R. & Schiller, H., 2007. The MERIS Case 2 water algorithm. *International Journal of Remote Sensing*, 28(3-4), pp.517–535.

Dupouy, C. et al., 2008. Bio-optical properties of the marine cyanobacteria Trichodesmium spp. *Journal of Applied Remote Sensing*, 2(023503), pp.1–17.

Fell, F. et al., 2003. Retrieval of chlorophyll concentration from MERIS measurements in the spectral range of sun-induced chlorophyll fluorescence. In *Proceedings of SPIE*. p. 116.

Field, C.B. et al., 1998. Primary Production of the Biosphere: Integrating Terrestrial and Oceanic Components. *Science*, 281(5374), p.237–240.

Giardino, C., Candiani, G. & Zilioli, E., 2005. Detecting Chlorophyll-a in Lake Garda Using TOA MERIS Radiances. *Photogrammetric Engineering & Remote Sensing*, 71(9), pp.1045–1051.

Gilerson, A. et al., 2007. Comparison of fluorescence retrieval algorithms using radiative transfer simulations and field measurements. In *IEEE International Conference on Geoscience and Remote Sensing, 2006.* IEEE, pp. 1312–1315.

Gilerson, A. et al., 2008. Fluorescence component in the reflectance spectra from coastal waters. II. Performance of retrieval algorithms. *Optics express*, 16(4), pp.2446–60.

Gilerson, A. et al., 2010. Algorithms for remote estimation of chlorophyll-a in coastal and inland waters using red and near infrared bands. *Optics express*, 18(23), pp.24109–25.

Gitelson, A., 1992. The peak near 700 nm on radiance spectra of algae and water: relationships of its magnitude and position with chlorophyll concentration. *International Journal of Remote Sensing*, 13(17), pp.3367–3373.

Gitelson, A.A. et al., 1999. Comparative reflectance properties of algal cultures with manipulated densities. *Journal of Applied Phycology*, 11(4), pp.345–354.

Gons, H.J., 1999. Optical teledetection of chlorophyll a in turbid inland waters. *Environmental Science & Technology*, 33(7), pp.1127–1132.

Gons, H.J., Auer, M.T. & Effler, S.W., 2008. MERIS satellite chlorophyll mapping of oligotrophic and eutrophic waters in the Laurentian Great Lakes. *Remote Sensing of Environment*, 112(11), pp.4098–4106.

Gordon, H.R., 2002. Inverse methods in hydrologic optics. *Oceanologia*, 44(1), pp.9–58.

Gordon, H.R., Brown, O.B. & Jacobs, M.M., 1975. Computed relationships between the inherent and apparent optical properties of a flat homogeneous ocean. *Applied optics*, 14(2), pp.417–427.

Gordon, R. et al., 1988. A semianalytic radiance model of ocean color. *Journal of Geophysical Research*, 93(D9), pp.10909–10924.

Gower, J.F.R., 1980. Observations of in situ fluorescence of chlorophyll-a in Saanich Inlet. *Boundary-Layer Meteorology*, 18(3), pp.235–245.

Gower, J.F.R., Doerffer, R. & Borstad, G.A., 1999. Interpretation of the 685nm peak in water-leaving radiance spectra in terms of fluorescence, absorption and scattering, and its observation by MERIS. *International Journal of Remote Sensing*, 20(9), pp.1771–1786.

Gregor, J. & Marsalek, B., 2004. Freshwater phytoplankton quantification by chlorophyll a: a comparative study of in vitro, in vivo and in situ methods. *Water research*, 38(3), pp.517–522.

Han, L. et al., 1994. The spectral responses of algal chlorophyll in water with varying levels of suspended sediment. *International Journal of Remote Sensing*, 15(18), pp.3707–3718.

Hu, C. et al., 2012. Dynamic range and sensitivity requirements of satellite ocean color sensors: learning from the past. *Applied optics*, 51(25), pp.6045–6062.

Hunter, P.D. et al., 2008. Spectral discrimination of phytoplankton colour groups: The effect of suspended particulate matter and sensor spectral resolution. *Remote Sensing of Environment*, 112(4), pp.1527–1544.

Huot, Y. & Babin, M., 2010. *Chlorophyll a Fluorescence in Aquatic Sciences: Methods and Applications* D.J. Suggett, O. Prášil, & M.A. Borowitzka, eds., Dordrecht: Springer Netherlands.

Huot, Y. et al., 2007. Does chlorophyll *a* provide the best index of phytoplankton biomass for primary productivity studies? *Biogeosciences Discussions*, 4(2), pp.707–745.

IOCCG, 2012. *Mission Requirements for Future Ocean-Colour Sensors*. Report No. 13.

IOCCG,1998. *Minimum requirements for an operational ocean-colour sensor for the open ocean*. Report No. 1.

Johnsen, G. & Sakshaug, E., 2007. Biooptical characteristics of PSII and PSI in 33 species (13 pigment groups) of marine phytoplankton, and the relevance for pulse-amplitude-modulated and fast-repetition-rate fluorometry. *Journal of Phycology*, 43(6), pp.1236–1251.

Kitchen, J.C. & Zaneveld, J.R.V, 1992. A Three-Layered Sphere Model of the Optical Properties of Phytoplankton. *Limnology and Oceanography*, 37(8), pp.1680–1690.

Kudela, R.M. et al., 2015. Application of hyperspectral remote sensing to cyanobacterial blooms in inland waters. *Remote Sensing of Environment*, 167, pp.196–205.

Kutser, T., 2009. Passive optical remote sensing of cyanobacteria and other intense phytoplankton blooms in coastal and inland waters. *International Journal of Remote Sensing*, 30(17), pp.4401–4425.

Kutser, T., Metsamaa, L. & Dekker, A.G., 2008. Influence of the vertical distribution of cyanobacteria in the water column on the remote sensing signal. *Estuarine, Coastal and Shelf Science*, 78, pp.649–654.

Lee, Z. & Carder, K.L., 2004. Absorption spectrum of phytoplankton pigments derived from hyperspectral remote-sensing reflectance. *Remote Sensing of Environment*, 89(3), pp.361–368.

Lee, Z. et al., 2011. An inherent-optical-property-centred approach to correct the angular effects in water-leaving radiance. *Applied optics*, 50(19), pp.3155–3167.

Letelier, M. & Abbott, M.R., 1996. An analysis of chlorophyll fluorescence algorithms for the moderate resolution imaging spectrometer (MODIS). *Remote Sensing of Environment*, 58(2), pp.215–223.

Lu, Y. et al., 2016. Sunlight induced chlorophyll fluorescence in the near-infrared spectral region in natural waters: Interpretation of the narrow reflectance peak around 761 nm. *Journal of Geophysical Research: Oceans*, 121(7), pp.5017–5029.

Lunetta, R.S. et al., 2014. Evaluation of cyanobacteria cell count detection derived from MERIS imagery across the eastern USA. *Remote Sensing of Environment*, 157, pp.24–34.

Matsushita, B. et al., 2015. A hybrid algorithm for estimating the chlorophyll-a concentration across different trophic states in Asian inland waters. *ISPRS Journal of Photogrammetry and Remote Sensing*, 102, pp.28–37.

Matthews, M.W., 2011. A current review of empirical procedures of remote sensing in inland and near-coastal transitional waters. *International Journal of Remote Sensing*, 32(21), pp.6855–6899.

Matthews, M.W., Bernard, S. & Robertson, L., 2012. An algorithm for detecting trophic status (chlorophyll-a), cyanobacterial-dominance, surface scums and floating vegetation in inland and coastal waters. *Remote Sensing of Environment*, 124, pp.637–652.

Matthews, M.W. & Odermatt, D., 2015. Improved algorithm for routine monitoring of cyanobacteria and eutrophication in inland and near-coastal waters. *Remote Sensing of Environment*, 156, pp.374–382.

Matthews, M.W. & Bernard, S., 2013. Characterizing the Absorption Properties for Remote Sensing of Three Small Optically-Diverse South African Reservoirs. *Remote Sensing*, 5, pp.4370–4404.

Matthews, M.W., 2014. Eutrophication and cyanobacterial blooms in South African inland waters: 10 years of MERIS observations. *Remote Sensing of Environment*, 155, pp.161–177.

Mckee, D. et al., 2007. Potential impacts of nonalgal materials on water-leaving Sun induced chlorophyll fluorescence signals in coastal waters. *Applied Optics*, 46(31), pp.7720–7729.

Meroni, M. et al., 2009. Remote sensing of solar-induced chlorophyll fluorescence: Review of methods and applications. *Remote Sensing of Environment*, 113(10), pp.2037–2051.

Mishra, S., Mishra, D.R. & Lee, Z., 2014. Bio-Optical Inversion in Highly Turbid and Cyanobacteria Dominated Waters. *IEEE Transactions on Geoscience and Remote Sensing*, 52(1), pp.375–388.

Moore, T.S. et al., 2014. An optical water type framework for selecting and blending retrievals from bio-optical algorithms in lakes and coastal waters. *Remote Sensing of Environment*, 143, pp.97–111.

Morel, A. & Bricaud, A., 1986. Inherent optical properties of algal cells including picoplankton: theoretical and experimental results. *Can. Bull. Fish. Aquat. Sci*, 214, pp.521–559.

Morel, A. & Prieur, L., 1977. Analysis of variations in ocean color. *Limnology and Oceanography*, 22(4), pp.709–722.

Moses, W.J. et al., 2012. Impact of signal-to-noise ratio in a hyperspectral sensor on the accuracy of biophysical parameter estimation in case II waters. *Optics express*, 20(4), pp.4309–4330.

Mouw, C.B. et al., 2015. Aquatic color radiometry remote sensing of coastal and inland waters: Challenges and recommendations for future satellite missions. *Remote Sensing of Environment*, 160, pp.15–30.

Neville, R. & Gower, J.F.R., 1977. Passive Remote Sensing of Phytoplankton via Chlorophyll α Fluorescence. *Journal of Geophysical Research*, 82(24), pp.3487–3493.

O'Reilly, J.E. et al., 1998. Ocean color chlorophyll algorithms for SeaWiFS. *Journal of Geophysical Research*, 103(C11), p.24937.

Odermatt, D. et al., 2012. Review of constituent retrieval in optically deep and complex waters from satellite imagery. *Remote Sensing of Environment*, 118, pp.116–126.

Odermatt, D. et al., 2012. MERIS observations of phytoplankton blooms in a stratified eutrophic lake. *Remote Sensing of Environment*, 126, pp.232–239.

Palmer, S.C.J. et al., 2014. Validation of Envisat MERIS algorithms for chlorophyll retrieval in a large, turbid and optically-complex shallow lake. *Remote Sensing of Environment*.

Palmer, S.C.J., Kutser, T. & Hunter, P.D., 2015. Remote sensing of inland waters: Challenges, progress and future directions. *Remote Sensing of Environment*, 157, pp.1–8.

Palmer, S. et al., 2013. Ultraviolet Fluorescence LiDAR (UFL) as a Measurement Tool for Water Quality Parameters in Turbid Lake Conditions. *Remote Sensing*, 5(9), pp.4405–4422.

Piskozub, J. & McKee, D., 2011. Effective scattering phase functions for the multiple scattering regime. *Optics express*, 19(5), pp.4786–4794.

Quibell, G., 1991. The effect of suspended sediment on reflectance from freshwater algae. *International Journal of Remote Sensing*, 12(1), pp.177–182.

Quibell, G., 1992. Estimating Chlorophyll Concentrations using Upwelling Radiance from Different Fresh-Water Algal Genera. *International Journal of Remote Sensing*, 13(14), pp.2611–2621.

Quinby-Hunt, M.S. et al., 1989. Polarized-light scattering studies of marine chlorella. *Limnology and Oceanography*, 34(8), pp.1587– 1600.

Quirantes, A. & Bernard, S., 2006. Light-scattering methods for modelling algal particles as a collection of coated and/or nonspherical scatterers. *Journal of Quantitative Spectroscopy and Radiative Transfer*, 100(1-3), pp.315–324.

Reynolds, C.S., 2006. *The Ecology of Phytoplankton*, New York: Cambridge University Press.

Richardson, L.L., 1996. Remote Sensing of Algal Bloom Dynamics. *BioScience*, 46(7), pp.492–501.

Ritchie, R.J., 2006. Consistent sets of spectrophotometric chlorophyll equations for acetone, methanol and ethanol solvents. *Photosynthesis research*, 89(1), pp.27–41.

Robertson Lain, L., Bernard, S. & Evers-King, H., 2014. Biophysical modelling of phytoplankton communities from first principles using two-layered spheres: Equivalent Algal Populations (EAP) model. *Optics express*, 22(14), pp.16745–16758.

Ruiz-Verdú, A. et al., 2008. An evaluation of algorithms for the remote sensing of cyanobacterial biomass. *Remote Sensing of Environment*, 112(11), pp.3996–4008.

Rundquist, D.C. et al., 1996. Remote Measurement of Algal Chlorophyll in Surface Waters: The Case for the First Derivative of Reflectance Near 690 nm. , 62(2), pp.195–200.

Ryan, J. et al., 2014. Application of the Hyperspectral Imager for the Coastal Ocean to Phytoplankton Ecology Studies in Monterey Bay, CA, USA. *Remote Sensing*, 6(2), pp.1007–1025.

Salama, M.S. et al., 2009. Deriving inherent optical properties and associated inversion-uncertainties in the Dutch Lakes. *Hydrol. Earth Syst. Sci*, 13, pp.1113–1121.

Santini, F. et al., 2010. A two-step optimization procedure for assessing water constituent concentrations by hyperspectral remote sensing techniques: an application to the highly turbid Venice lagoon waters. *Remote Sensing of Environment*, 114(4), pp.887–898.

Sathyendranath, S. & Platt, T., 1997. Analytic model of ocean color. *Appl. Opt.*, 36(12), pp.2620–2629.

Sayers, M.J. et al., 2015. A new method to generate a high-resolution global distribution map of lake chlorophyll. *International Journal of Remote Sensing*, 36(7), pp.1942–1964.

Sayers, M. et al., 2016. Cyanobacteria blooms in three eutrophic basins of the Great Lakes: a comparative analysis using satellite remote sensing. *International Journal of Remote Sensing*, 37(17), pp.4148–4171.

Schalles, J.F. et al., 1998. Estimation of chlorophyll a from time series measurements of high spectral resolution reflectance in an eutrophic lake. *Journal of Phycology*, 34(2), pp.383–390.

Seppälä, J. et al., 2007. Ship-of-opportunity based phycocyanin fluorescence monitoring of the filamentous cyanobacteria bloom dynamics in the Baltic Sea. *Estuarine, Coastal and Shelf Science*, 73(3-4), pp.489–500.

Simis, S.G.H. et al., 2007. Influence of phytoplankton pigment composition on remote sensing of cyanobacterial biomass. *Remote Sensing of Environment*, 106(4), pp.414–427.

Simis, S.G.H. et al., 2012. Optimization of variable fluorescence measurements of phytoplankton communities with cyanobacteria. *Photosynthesis Research*, 112(1), pp.13–30.

Stramski, D., Bricaud, A. & Morel, A., 2001. Modeling the inherent optical properties of the ocean based on the detailed composition of the planktonic community. *Applied Optics*, 40(18), pp.2929–2945.

Stramski, D., Babin, M. & Wozniak, S.B., 2007. Variations in the optical properties of terrigenous mineral-rich particulate matter suspended in seawater. *Limnology and Oceanography*, 52(6), pp.2418–2433.

Svensen, Ø., Frette, Ø. & Erga, S.R., 2007. Scattering properties of microalgae: the effect of cell size and cell wall. *Applied Optics*, 46, pp.5762–5769.

Tao, B. et al., 2015. A novel method for discriminating Prorocentrum donghaiense from diatom blooms in the East China Sea using MODIS measurements. *Remote Sensing of Environment*, 158, pp.267–280.

Tao, B. et al., 2013. Influence of bio-optical parameter variability on the reflectance peak position in the red band of algal bloom waters. *Ecological Informatics*, 16(April 2016), pp.17–24.

Tomlinson, M.C. et al., 2016. Relating chlorophyll from cyanobacteria-dominated inland waters to a MERIS bloom index. *Remote Sensing Letters*, 7(2), pp.141–149.

Vaillancourt, R.D. et al., 2004. Light backscattering properties of marine phytoplankton: relationships to cell size, chemical composition and taxonomy. *Journal of Plankton Research*, 26(2), pp.191–212.

Verpoorter, C. et al., 2014. A Global Inventory of Lakes Based on High-Resolution Satellite Imagery. *Geophysical Research Letters*, 41(18), pp.6396–6402.

Volten, A.H. et al., 1998. Laboratory Measurements of Angular Distributions of Light Scattered by Phytoplankton and Silt. *Limnology and Oceanography*, 43(6), pp.1180–1197.

Wang, G. et al., 2016. Retrieving absorption coefficients of multiple phytoplankton pigments from hyperspectral remote sensing reflectance measured over cyanobacteria bloom waters. *Limnology and Oceanography: Methods*, 14(7), pp.432–447.

Werdell, P.J. & Bailey, S.W., 2005. An improved in-situ bio-optical data set for ocean color algorithm development and satellite data product validation. *Remote Sensing of Environment*, 98(1), pp.122–140.

Whitmire, A.L. et al., 2010. Spectral backscattering properties of marine phytoplankton cultures. *Optics Express*, 18(14), pp.1680–1690.

Witkowski, K. et al., 1998. A Light-Scattering Matrix for Unicellular Marine Phytoplankton. *Limnology and Oceanographyology*, 43(5), pp.859–869.

Wynne, T.T. et al., 2008. Relating spectral shape to cyanobacterial blooms in the Laurentian Great Lakes. *International Journal of Remote Sensing*, 29(12), pp.3665–3672.

Wynne, T. & Stumpf, R., 2015. Spatial and Temporal Patterns in the Seasonal Distribution of Toxic Cyanobacteria in Western Lake Erie from 2002–2014. *Toxins*, 7(5), pp.1649–1663.

Zhang, Y. et al., 2012. Effect of phytoplankton community composition and cell size on absorption properties in eutrophic shallow lakes: field and experimental evidence. *Optics express*, 20(11), pp.11882–11898.

Zhou, J. et al., 2008. Retrieving quantum yield of sun-induced chlorophyll fluorescence near surface from hyperspectral in-situ measurement in productive water. *Optics express*, 16(22), pp.17468–83.

Zhou, W. et al., 2012. Variations in the optical scattering properties of phytoplankton cultures. *Optics express*, 20(10), pp.11189–11206.